Supplementary Figure 1

a

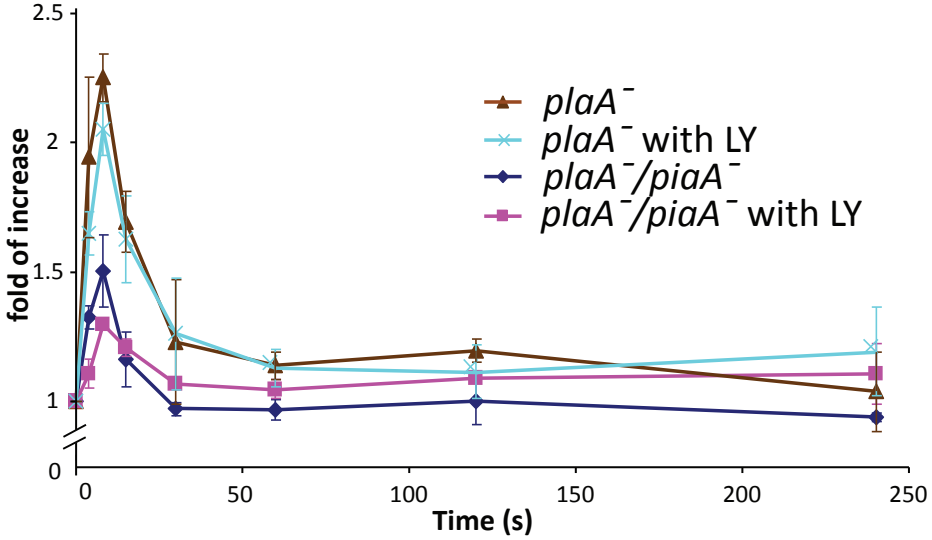

b

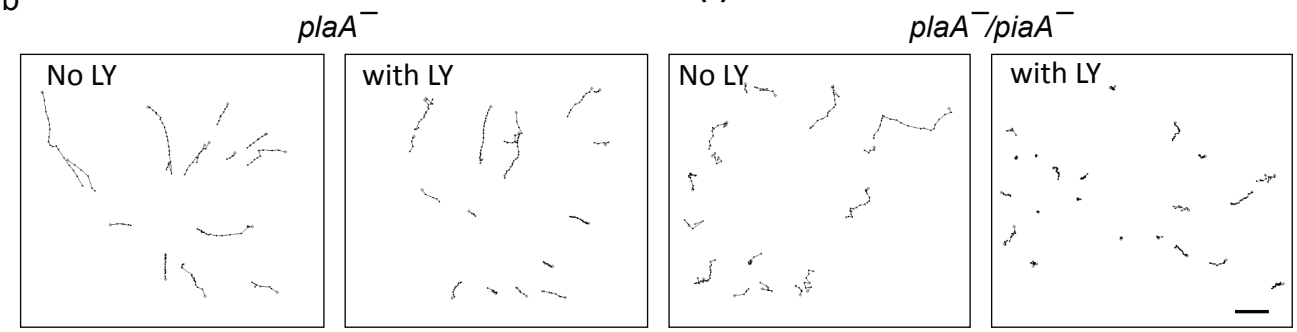

c

60X fluorescence	*plaA*⁻	*plaA*⁻ with LY	*plaA*⁻/*piaA*⁻	*plaA*⁻/*piaA*⁻ with LY
chemotaxis speed (μm/min)	5.69 ±0.65	2.97 ±0.41	1.94 ±0.52	0.56±0.18
motility speed (μm/min)	6.74 ±0.69	4.54 ±0.45	5.81 ±0.74	2.44 ±0.35
chemotaxis index	0.82 ±0.03	0.66 ±0.06	0.37 ±0.08	0.18±0.06

10X phase	*plaA*⁻	*plaA*⁻ with LY	*plaA*⁻/*piaA*⁻	*plaA*⁻/*piaA*⁻ with LY
chemotaxis speed (μm/min)	1.67 ±0.24	1.34 ±0.42	1.22 ±0.42	0.49±0.20
motility speed (μm/min)	4.06 ±0.20	3.30 ±0.44	3.92 ±0.47	2.75 ±0.53
chemotaxis index	0.40 ±0.07	0.38 ±0.07	0.31 ±0.09	0.21±0.04

10X phase	*sGC*⁻	*sGC*⁻ with LY	*sGC*⁻/*plaA*⁻/*piaA*⁻	*sGC*⁻/*plaA*⁻/*piaA*⁻ with LY
chemotaxis speed (μm/min)	2.32 ±0.24	1.41 ±0.62	0.58 ±0.15	0.13±0.07
motility speed (μm/min)	4.65 ±0.28	3.63 ±1.10	3.24 ±0.44	1.53 ±0.36
chemotaxis index	0.47 ±0.03	0.38 ±0.08	0.21 ±0.02	0.08±0.04

d

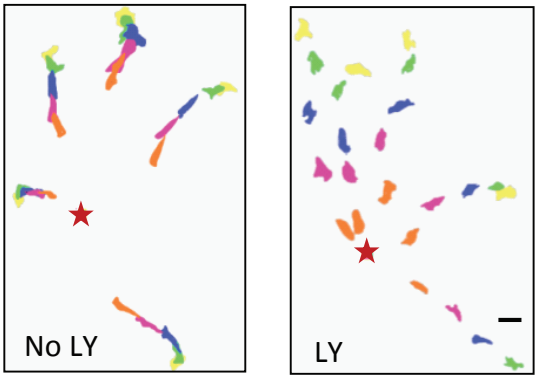

e

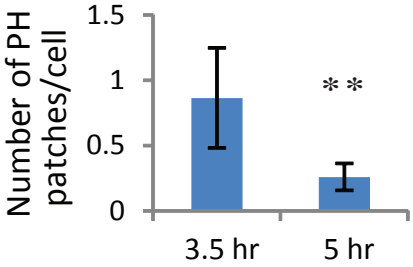

Supplementary Figure 1. The effects of simultaneous blockade of PLA2, TorC2, and PI3K.

(a) Biochemical measurement of F-actin after global cAMP stimulus. *Dictyostelium* cells were developed for 5 hours, washed, and stimulated with 1 μM cAMP at 0 s. Samples were taken at the indicated time points, fixed, and stained with TRITC-phalloidin. The amount of F-actin was proportional to the phalloidin fluorescence [1]. (b) Centroid tracks of *plaA*- and *plaA*-/*piaA*- cells treated with 30 μM LY or control volume of DMSO. These are derived from the same time-lapse videos as in Figure 1b. Scale bar: 20 μm. (c) Summary of chemotaxis speed (the distance toward the micropipette divided by time), motility speed (total distance traveled divided by time), and chemotaxis index (the cosine of the angle between the direction of movement and the direction from the start point to the micropipette) of different cell lines and acquisition conditions. *Note that chemotaxis index may not correlate well with directional sensing in cells with poor motility. In immobilized *plaA*-/*piaA*-/+LY cells, the RBD-GFP still responded directionally to the gradient, suggesting that cells are capable of sensing the gradient (Fig. 1c). Under very low motility speed, changes in cell morphology significantly interfere with calculation of cell position change, making the chemotactic index a poor indicator of directionality. This factor may contribute to the low chemotactic index in cells with multiple signaling pathways blocked despite preservation of directional sensing. (d) Chemotaxis of cells developed for 3.5 hours treated with 30 μM LY or control volume of DMSO. Cell migration toward the tip of a micropipette filled with 1 μM cAMP (red stars) was recorded at 15 s interval. Five representative cells in each movie were outlined and traced every 5 frames. Scale bar: 20 μm. With LY, the chemotaxis speed increased from 1.38 ± 0.53 to 2.32 ± 0.51 μm min^{-1}, motility speed from 3.84 ± 0.31 to 4.74 ± 0.29 μm min^{-1}, and chemotaxis index from 0.35 ± 0.11 to 0.45 ± 0.15 μm min^{-1}. (e) Quantification of the number of PH patches per cell (mean ± s.d.) for randomly migrating cells after 3.5 hour (n = 48) and 5 hour (n = 36) of development. **p<0.001 (two-tailed Student's t-test)

Supplementary Figure 2

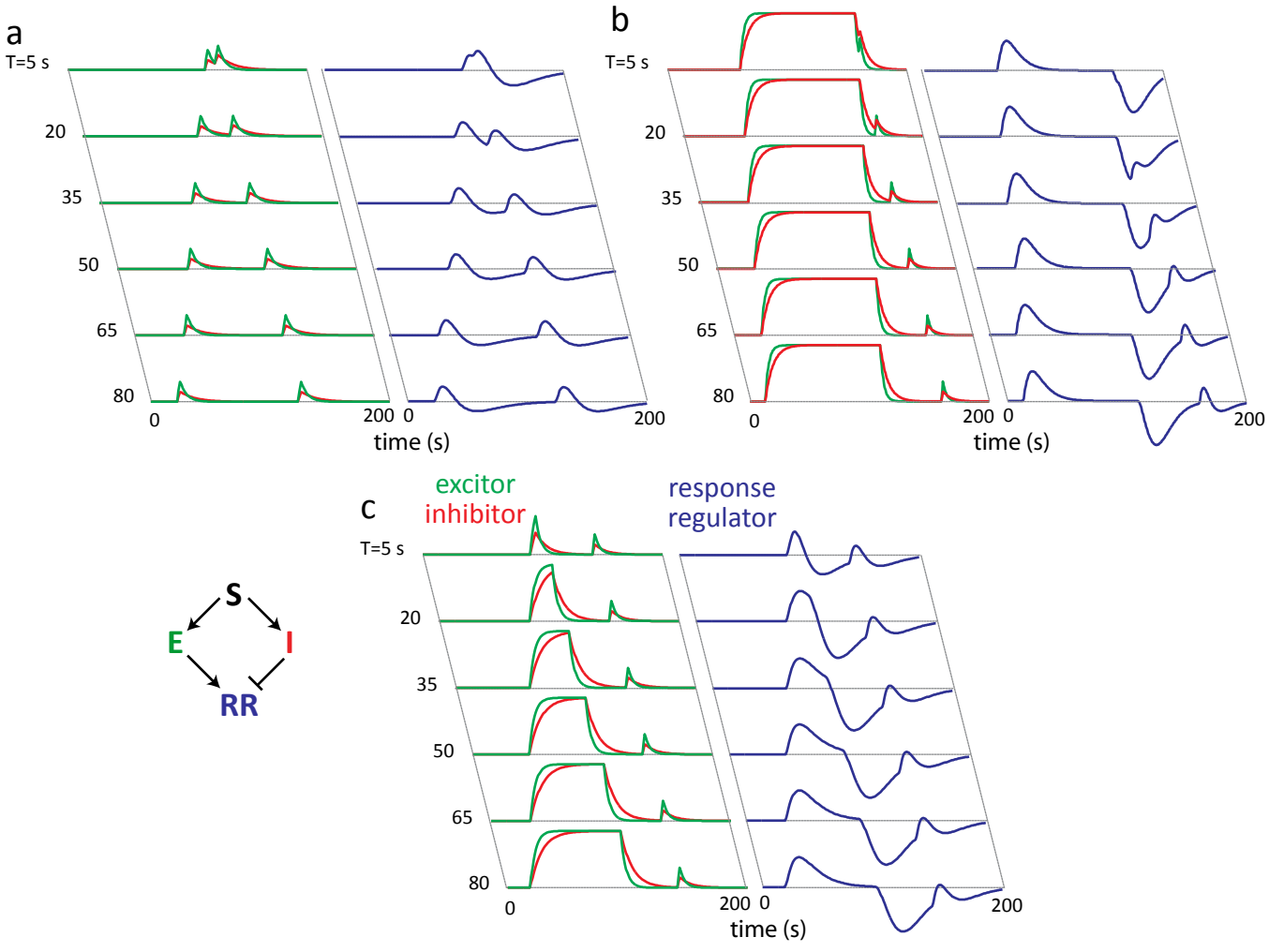

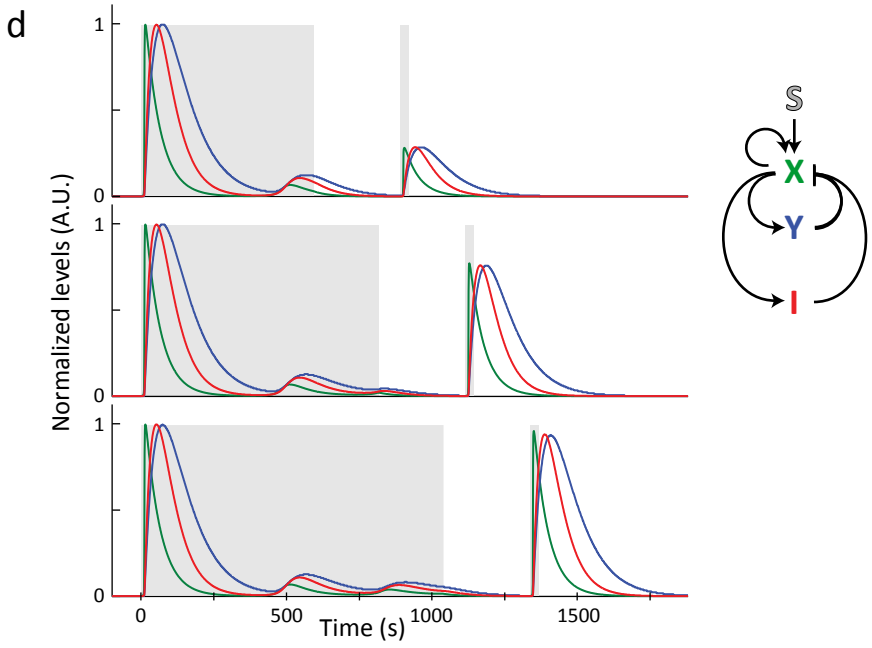

Supplementary Figure 2. Simulations of double stimulation protocols.
(a-c) Time traces of the excitor (E), inhibitor (I) and response regulator (RR) for the LEGI-BEN model for the various stimuli of Fig. 3a, b. (a) The time between the two 2 s pulses was varied. (b) The time between the initial 150 s pulse and the second 2 s pulse was varied. (c) The length of the first pulse was varied. (d) Time traces of the activator (X), local inhibitor (Y) and global inhibitor (I) for the BENGI model for the various stimuli (shaded regions) of Fig. 3b, where the length of the first pulse was varied.

Supplementary Figure 3

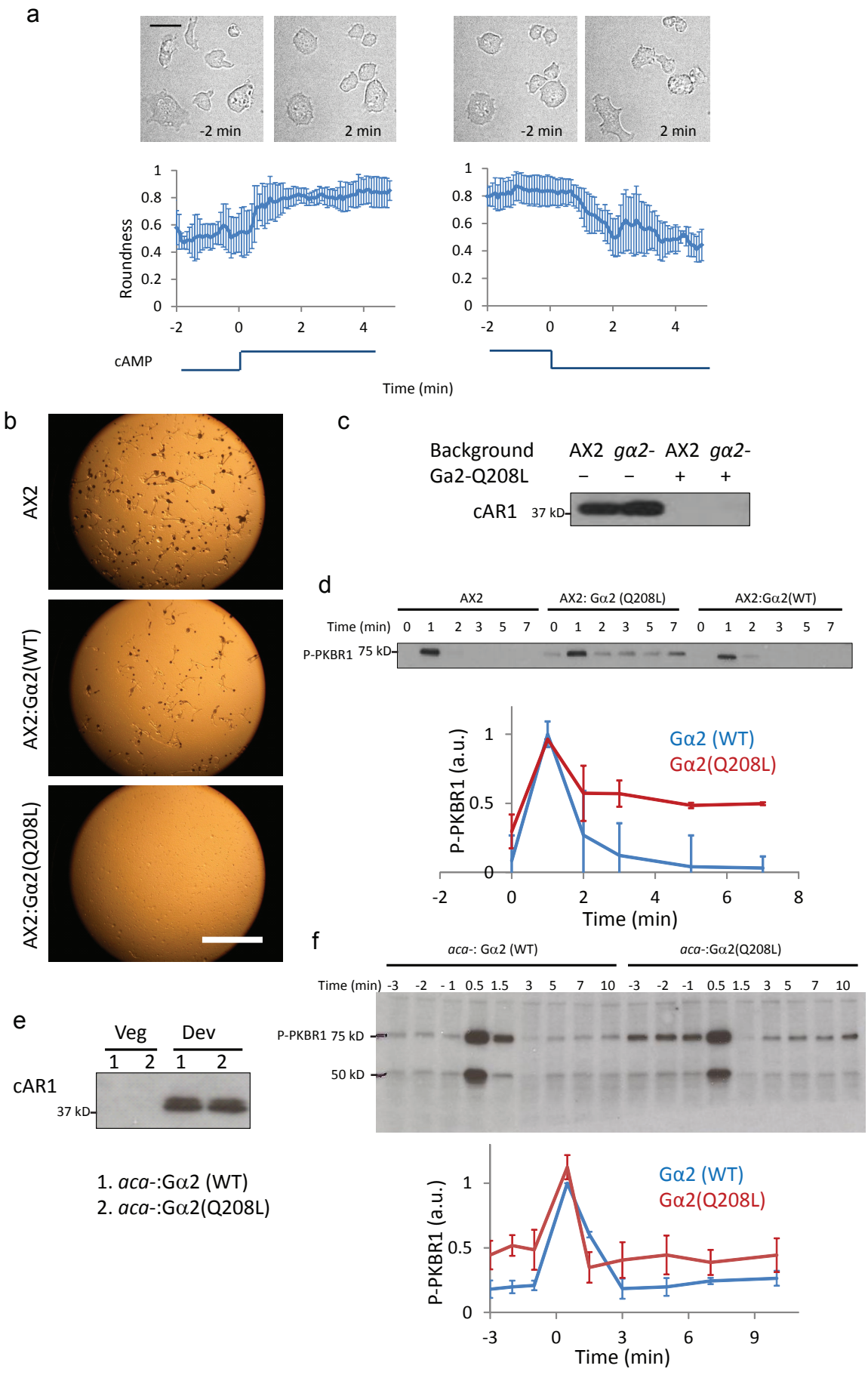

Supplementary Figure 3. Response of *gβ*- cells to stimulus and behaviors of cells expressing constitutively active Gα2 mutant and rescue in *aca*- cells.
(a) Morphology changes of *gβ*- cells upon 1 μM cAMP stimulation and removal. *gβ*- cells expressing cAR1 were developed for 5.5hr before they were loaded to ibidi chamber (http://ibidi.com/). Movies were recorded at 5 s intervals. Representative cell images were shown on the top. Cell roundness was calculated using particle analysis function in ImageJ (mean ± s.d. of n = 7 cells). Scale bar: 15 μm. (b-f) Suppression of development by constitutively active Gα2 mutant and rescue in *aca*- cells. (b) Suppression of fruiting body formation on DB agar by the expression of the constitutively active Gα2(Q208L) but not wild-type Gα2 in wild-type *Dictyostelium* cells (AX2 strain). 10^7 cells were washed in development buffer twice before plating on a 3.5 ml dish containing 1% DB agar [2]. Images were taken at 24 hours. Scale bar: 2 mm. (c) Gα2(Q208L) suppressed the expression of the cAMP receptor, cAR1, during development. AX2 and *gα2*(-) cells were developed by cAMP pulsing in development buffer, lysed, and probed with anti-cAR1 antibody. (d) Gα2(Q208L) caused high basal level of PKBR1 phosphorylation in wild-type cells. Top: AX2 cells alone or expressing either Gα2(Q208L) or wild-type Gα2 were developed for 6 hours, washed, and stimulated with 1 μM cAMP at 0 min. Samples were taken at indicated time points and probed with anti–phospho-AL antibody[2]. Bottom: Quantitative densitometry of phosphorylated PKBR1 normalized to the peak intensity of the AX2 cell samples (mean ± s.d. of n = 3 experiments). (e) Blockade of cAR1 expression by Gα2(Q208L) is reversed in *aca*- cells, suggesting that adenylate cyclase may also be persistently activated. Vegetative (growth-stage, non-developed) and developed *aca*- cells expressing Gα2(WT) and Ga2(Q208L) were lysed and probed with anti-cAR1 antibody. (f) Gα2(Q208L) caused high basal level of PKBR1 phosphorylation in *aca*- cells. Top: *aca*- cells expressing either wild-type Gα2 or Gα2(Q208L) were developed for 6 hours, washed, and stimulated with 1 μM cAMP at 0 min. Samples were taken at indicated time points and probed with anti–phospho-AL antibody[2]. Bottom: Quantitative densitometry of phosphorylated PKBR1 normalized to the peak intensity of the *aca*- cells expressing Gα2(WT) (mean ± s.d. of n = 2 experiments).

Supplementary Figure 4

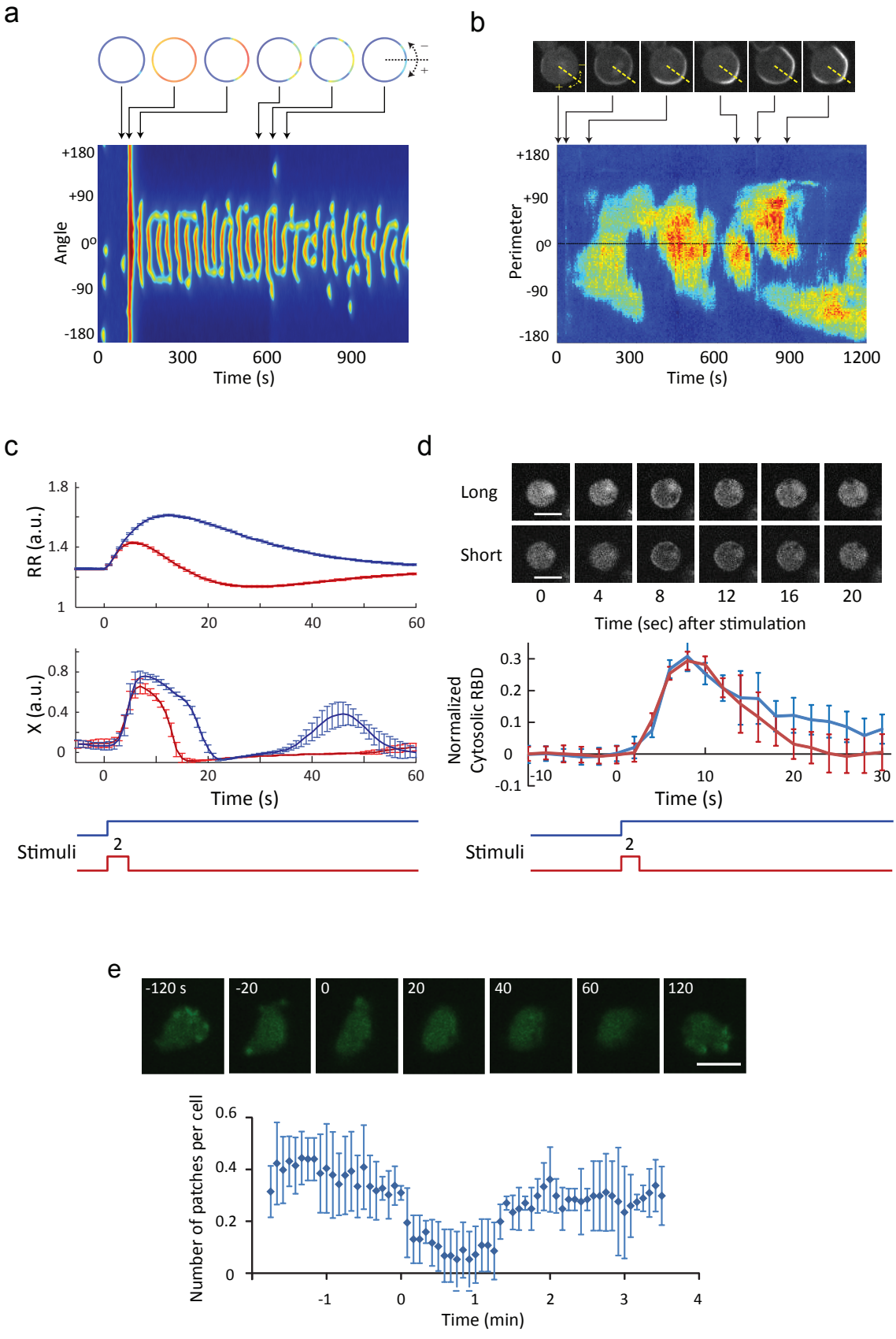

Supplementary Figure 4. Simulations and experiments of the LEGI-BEN model. (a) Simulation of LEGI-BEN responding to the introduction of a gradient at 100 s followed by a global stimulus at 600 s. The protocol and kymograph are as in Fig. 5a but with a steeper gradient. (b) Kymograph showing the "dancing" crescent of a latrunculin-treated *Dictyostelium* cell expressing PH-GFP. A gradient was initiated at 15 s, and global stimuli of 1 nM, 10 nM, and 100 nM cAMP were added at 450 s, 540 s, and 730 s respectively. Representative cell images were shown on the top panel. Dotted line indicates the direction of the tip of the micropipette filled with cAMP. The kymograph levels represent the ratio of local cortical PH-GFP around the perimeter of the cell, over mean cytosolic intensity. The analysis was derived from the same experiment as in Figure 5b using a cell closer to the tip of the micropipette. (c) Simulated responses of LEGI-BEN to short and long stimuli (mean ± s.d. of n=10 simulations, each). (d) Ras activation in cells responding to short and long stimuli. *Dictyostelium* cells expressing RBD-GFP were stimulated with either 2 s or continued cAMP at 0 s. The graph shows the cytosolic decrease of RBD-GFP normalized to pre-stimulus level of fluorescence (mean ± s.d. of n=20 cells). Representative cell images were shown on the top panel. Scale bar: 10 μm. (e) RBD-GFP response to removal of stimulus. *Dictyostelium* cells expressing RBD-GFP were developed and loaded to a microfluidic chamber and perfused with 1 μM cAMP in development buffer for 6 min, followed by switch to buffer without cAMP. The flow rate was kept constant during the entire experiment. Top: Representative images from time-lapse videos of cAMP removal at 0 min. Bottom: Quantitation of RBD activity (mean ± s.d. of n = 4 movies, each containing 7-16 cells). Scale bar: 10 μm.

Supplementary Figure 5

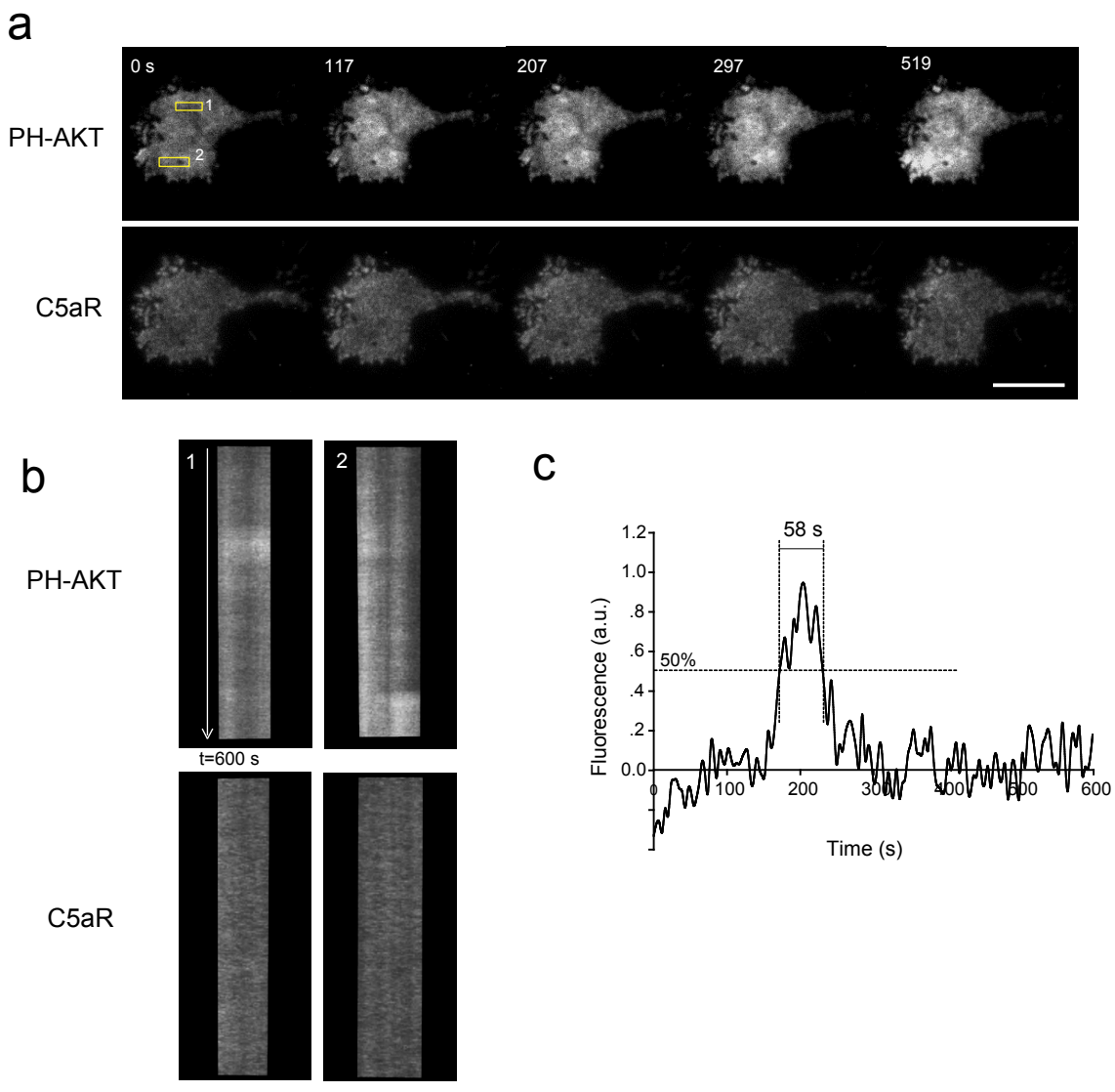

Supplementary Figure 5. Spontaneous flashes of PH-Akt-GFP in human neutrophils.

(a) Frames from a TIRF time-lapse video (Supplementary Movie 2, images captured every 3 s) of an HL-60 cell co-expressing PH-Akt-GFP and C5aR-RFP immobilized by JLY cocktail showed dynamic flashes of PH-Akt-GFP throughout the basal membrane that were 2-5 μm in diameter. The membrane marker C5aR-RFP did not show corresponding changes in intensity. Scale bar: 10 μm. (b) T-stacks for the two regions (boxes 1 and 2) in the same cells as in (a). T-stacks are 3D kymographs created by stacking all the frames of the TIRF time-lapse video [3]. (c) Fluorescence intensity of box 1 in (b) plotted as a function of time.

Supplementary Table 1: Model parameters

Local excitation, global inhibition (LEGI)					
k_e	0.231 s^{-1}	k_{-e}	0.231 s^{-1}		
k_i	0.1 s^{-1}	k_{-i}	0.1 s^{-1}		
k_r	0.1 s^{-1}	k_{-r}	0.08 s^{-1}		
D_I	1 $\mu m^2/s$				
Excitable network (BEN)					
D_X	1.86 $\mu m^2/s$	D_Y	4.77 $\mu m^2/s$		
k_{XX}	3.16 s^{-1}	k_{XY}	0.0236 s^{-1}		
k_{-X}	2.87 s^{-1}	k_{-Y}	0.11 s^{-1}		
k_M	0.32	B	−0.063		
k_{YX}	10.65 s^{-1}	R_{init}	1.25		
k_{UX}	0.8 s^{-1}	λ	1		
BENGI [4, 5]					
D_X	4.0×10^{-7}	D_Y	2.8×10^{-6}	D_I	4.0
k_{-X}	2.0×10^{-2} s^{-1}	k_{-Y}	1.3×10^{-2} s^{-1}	k_{-I}	3.0×10^{-2} s^{-1}
k_X	1.0×10^{-1}	k_{My}	2.0×10^{-1}	k_{Mx}	5.0×10^{-4}
k_I	3.0×10^{-2} s^{-1}	k_{XY}	7.0×10^{-3} s^{-1}		
k_U	2.0×10^{-2} s^{-1}	k_N	0.01-0.2		

Supplementary References

1. Chen, L. *et al.* Two phases of actin polymerization display different dependencies on PI(3,4,5)P3 accumulation and have unique roles during chemotaxis. *Mol Biol Cell* **14**, 5028-5037 (2003).
2. Cai, H., Huang, C.H., Devreotes, P.N. & Iijima, M. Analysis of chemotaxis in dictyostelium. *Methods Mol Biol* **757**, 451-468 (2012).
3. Huang, C.H., Tang, M., Shi, C., Iglesias, P.A. & Devreotes, P.N. An excitable signal integrator couples to an idling cytoskeletal oscillator to drive cell migration. *Nat Cell Biol* **15**, 1307-1316 (2013).
4. Meinhardt, H. Orientation of chemotactic cells and growth cones: models and mechanisms. *J Cell Sci* **112 (Pt 17)**, 2867-2874 (1999).
5. Neilson, M.P. *et al.* Chemotaxis: a feedback-based computational model robustly predicts multiple aspects of real cell behaviour. *PLoS Biol* **9**, e1000618 (2011).